Structural and Optical Characterization of Nanocrystalline SnSe Thin Film

Keyur S. Hingarajiya[#], K. D. Patel[*] and G. K. Solanki[*]

[#]*R. G. Shah Science College, Vasna, Ahmedabad-382460, Gujarat,India.*

[*]*Dept. of Physics, S. P. University, V. V. Nagar-388120, Gujarat,India.*

***Abstract*--Structural and optical properties of nanocrystalline SnSe thin film confer in this paper. For that purpose Nanocrystalline thin film of SnSe was deposited at room temperature having thickness 1µm, 2µm, 3µm and 4µm. Structural and optical properties studied by XRD, TEM, AFM, and Uv-Vis- Nir spectroscopy methods of all thin films. From these studied we found there is a strong effect of thickness on structural and optical properties of Nanocrystalline SnSe thin film.**

***Key words*: Nanocrystalline, thin film, XRD, AFM**

I. INTRODUCTION

Semiconductor nanostructures are of current interest due to the variation of their bulk properties when their characteristic dimensions become smaller than the mean free path of the carriers [1-3]. A key aspect of semiconductors in a nanostructured form is the modification of the energy levels and the density of states owing to the confinement of the charge carriers. The charge carriers are localized in nanostructures and this leads to a blue shift in the band gap [4,5]. Semiconductor nano materials exhibit size-dependent electronic band gap energies [6], melting temperatures [7], soild-solid phase transition temperatures [8] and pressures [9]. These properties of nanocrystals make them an interesting category of materials from photovoltaic, photoelectrochemical, electrochemical and nanoelectronic devices point of view [10-13]. Semiconductor compounds such as tin selenide (SnSe), a narrow band gap semiconductor [14], has attracted a lot of attention [14–22] in the last years due its great technological interest as optical and optoelectronic materials [22,23]. SnSe is widely used as holographic recording systems, infrared electronic and memory switching devices [23,24]. It is also used in photoelectrical cells, decreasing the photocorrosion process [23]. Keeping all these thing in mind, Nanocrystalline thin film of SnSe was deposited by spin coating having thickness 1µm, 2µm, 3µm and 4µm and its structural and optical properties were studied by XRD, TEM, AFM and UV-VIS-NIR spectroscopy methods.

II. EXPERIMENTAL

Tin salt ($SnCl_2 \cdot 2H_2O$), gray selenium powder (Se), ammonia buffer (p_H=11), and sodium sulfite (Na_2So_3) were used in our experiments. All chemicals were purchased from ALFA AESAR Company having 99.99% purity. Thin film deposition process was divided in to four steps as discussed below.

In the first step $SnCl_2 \cdot 2H_2O$ was dissolved in double distilled water and ammonia buffer is added drop wise to obtain an alkaline media of p_H =11. Sodium selenosulfate, which was used as a source of selenide ions for the purpose of this study, is commercially unavailable substance because it is relatively instable, especially upon exposure to light and it has to be freshly prepared prior to the thin film deposition process. Hence in second step we prepared the solution of sodium selenosulfate by adding gray selenium to a hot solution of sodium sulfite. The resulting heterogeneous solution was stirred for 10h at 373K by magnetic stirrer and afterwards the excess of gray selenium was filtered. The preparation of sodium selenosulfate solution is based on the following redox process.

$$Se_{(S)} + Na_2So_{3(aq)} \rightarrow Na_2SeSo_{3(aq)}$$

In the third step prepared solution of Sodium selenosulfate and solution of $SnCl_2 \cdot 2H_2O$ were mixed that results in to precipitation of Nanocrystalline SnSe formed in mixed solution by following the reaction,

$$HSe^- + OH^- \rightarrow Se^{-2} + H_2O$$
$$SeSo_3^{-2} + OH^- \rightarrow HSe^- + So_4^{-2}$$
$$Sn^{+2} + Se^{-2} \rightarrow SnSe$$

The chemical deposition of tin selenide films described in this paper was based on two important properties of selenosulphate. One is its complexing ability, much like the well known complexing ability of thiosulphate a costly compound than selenosulphate. Tin selenosulphate complexes are formed in excess of selenosulphate. The other one is the ability of selenosulphate to gradually release selenide ions upon hydrolytic decomposition in alkaline media. The released selenide ions then combine with the tin ions released from the tin selenosulphate complexes upon hydrolysis and finally precipitating in to Nanocrystalline SnSe. In the fourth step these precipitates were filtered and deposited on to glass

substrates by spin coating unit at 500 rpm to get SnSe thin films having thicknesses 1µm, 2µm, 3µm and 4µm.

First chemical compositional analyses were carried out using an energy dispersive analysis by X-rays setup (EDAX). Structural characterization of prepared thin film was carried out by XRD (Model: D2 PHASER Xray Diffraction Analyzer make: Bruker), TEM(Model : Tecnai 20, make : Philips, Netherlands), AFM(VEECO,U.S.A).Optical measurements were carried out in the wave length range of 200nm to 2500nm (perkin elmer spectrometer).

III. RESULTS AND DISCUSSION

A. EDAX

The EDAX of thin films was carried out using the electron microscope. The result of EDAX is shown in figure 1. Thus all thin films have been found to be nearly stoichiometric in nature without any impurities

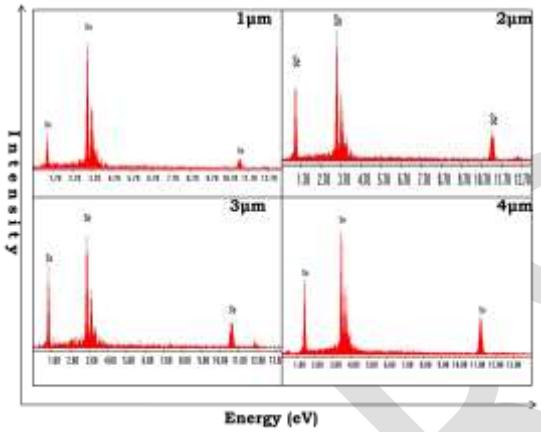

Fig. 1 EDAX result of Nanocrystalline SnSe thin films.

B. XRD

XRD pattern provided information about phase of the Nano material as well as the particle size. The structural properties of the deposited Nanocrystalline SnSe thin film have been investigated by XRD technique using CuKα radiation.

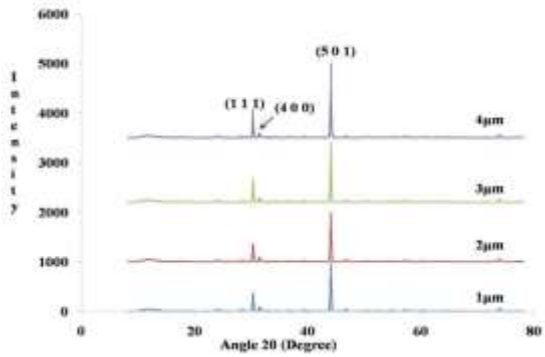

Fig. 2 XRD result of Nanocrystalline SnSe thin films.

Figure 2 shows the x-ray diffraction pattern of SnSe thin films. The XRD pattern exhibit sharp peaks at 26.62°,27.35° and 42.66° corresponding to the (111), (400) and (501) planes[25]. These sharp peaks conform the crystalline phase of thin films. All these peaks correspond to the orthorhombic phase thus the prepared thin films can be said to exhibit orthorhombic structure. The lattice parameters value a, b and c has been calculated and shown in table 1 which are in good agreement with the JCPDS data (32-1382).

The average size of particle and micro strain have been obtained from the x-ray diffraction pattern using the Scherrer's formula [26]

$$t = \frac{k\lambda}{\beta\cos\theta} \qquad \varepsilon = \frac{\beta_{2\theta}\cos\theta}{4}$$

Where, t is the particle size, ε is the micro strain, k is a constant taken to be 1, β is the full width at half maximum (FWHM) and λ is the wave length of the x-rays. The obtained average particle size values and micro strain of the prepared thin films are shown in table 1. It is found that as the film thickness is increased particle size is also increased and micro strain decreased. These results shows as film thickness increased crystallanity of thin films increased.

However, above mentioned method for determining the particle size and micro strain is valid only when the interfacial stress does not contribute. However, in those cases where both interfacial stress and particle size lead to broadening of the diffraction peaks, a more comprehensive method must be used to look in to their contributions. The most common method used to determine particle size and accompanying micro strain in such cases is Hall- Williamson method [15-17].

$$\frac{\beta_{2\theta}\cos\theta}{\lambda} = \frac{1}{t} + \frac{4\varepsilon\sin\theta}{\lambda}$$

From a Hall- Williamson plot as shown in figure 3 one can evaluate the contribution of micro strain and particle size to the XRD line broadening as shown in table 1.

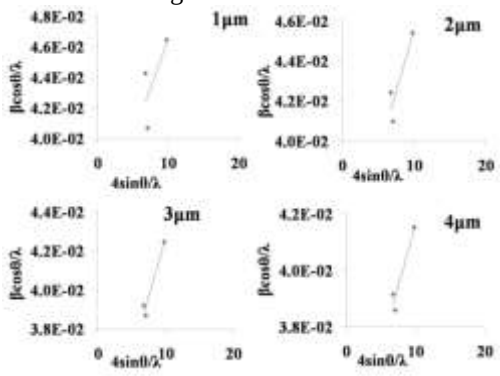

Fig. 3 Hall- Williamson plot of Nanocrystalline SnSe thin films.

Table 1: XRD results of particle size, microstrain and dislocation density of Nanocrystalline SnSe thin films.

SnSe thin film	Scherer's method for preferred orientation		Hall Williamson Plot	
	Particle Size nm	Micro strain $X10^{-3}$	Particle Size nm	Micro strain $X10^{-3}$
1µm	10.80	1.79	11.16	1.27
2µm	11.01	1.74	11.36	1.23
3µm	12.80	1.63	13.22	1.19
4µm	14.41	1.50	14.08	0.99

C. TEM

Fig. 4 and 5 shows TEM image and SAEDP of thin films.

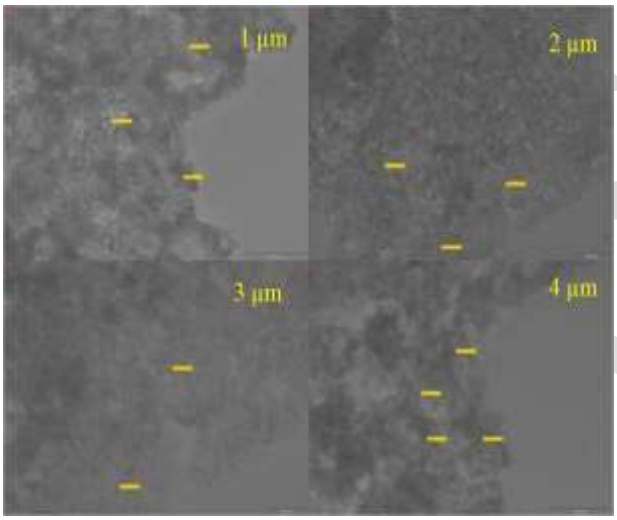

Fig. 4 TEM photograph of Nanocrystalline SnSe thin films.

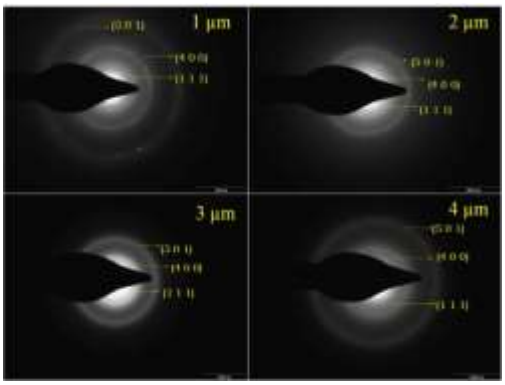

Fig. 5 SAEDP of Nanocrystalline SnSe thin films.

The TEM morphology shows particles have spherical shape. Particle sizes determined from Fig. 4 ranges between 10 – 20 nm. It is observed from figure 4 that as the thickness increased particle size increased. The nature of these diffraction patterns (fig. 5) confirm that all thin films of SnSe are polycrystalline having some texture like nature due to the appearance of distinct diffraction spots. Actually when the grains are continuously distributed, continuous and sharp rings are observed. When grains are randomly and partially continuous or there are only few grains/crystallites or the combination of both, then the ring pattern with spots is observed and it is said to be poor crystalline in nature. As in present case it is observe that the amount of spots are being reduced with increase in film thickness. Therefore, one can conclude that in as 1µm thickness thin film there is a possibility of discontinuous deposition of single grains and the cluster of grains and hence discontinuous ring pattern with spots are observed. However as the thickness is increased, films tends to be continuous and ring pattern with less spots are observed. Also this diffraction pattern shows (111), (400) and (501) reflections which are corresponding to the orthorhombic phase of SnSe nanocrystallites and there by matching with the XRD pattern.

D. AFM

Figure 6 shows obtained 2D and 3D AFM micrographs for SnSe thin films. AFM micrographs shows surface quality was improve with film thickness. Results obtained from line analysis are summarized in table 2.

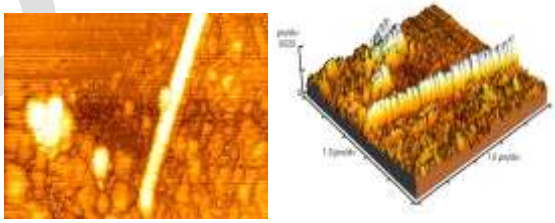

(i) 1µm

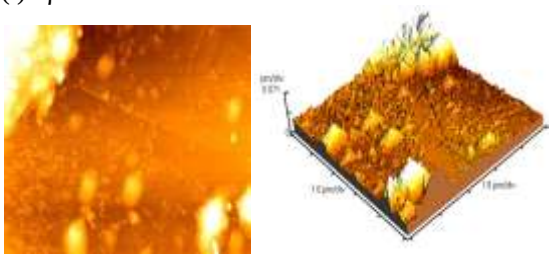

(ii) 2µm

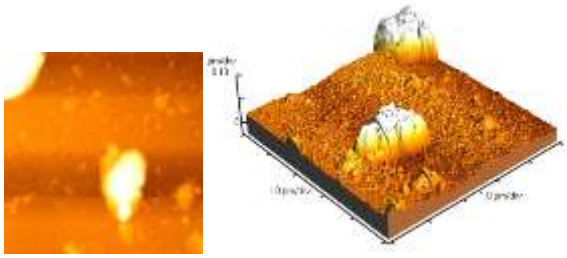

(iii) 3µm

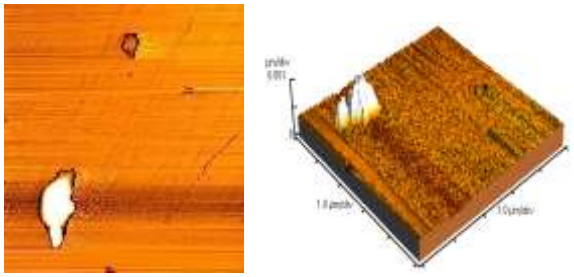

(iv) 4µm

Fig. 6 (i to iii) : 2D and 3D AFM micropraphs of Nanocrystalline SnSe thin films.

Table 2: roughness parameters of Nanocrystalline SnSe thin films.

Thin films	R_{p-v} (nm)	Roughness		Mean H_t (nm)	Median H_t (nm)	Peak R_p (nm)	Valley R_v (nm)
		Rms R_q (nm)	Ave. R_a (nm)				
1µm	49.37	12.54	9.88	17.20	12.25	34.11	-15.26
2µm	32.51	6.93	5.00	17.20	16.13	21.62	-10.89
3µm	39.91	6.61	4.19	17.12	15.53	28.73	-11.18
4µm	40.39	7.16	3.97	17.21	15.41	33.25	-7.14

E. UV-VIS- NIR spectroscopy

From the transmission data , the absorption coefficient (α), are calculated using the relation

$$\alpha = \frac{1}{d}\ln\left(\frac{1}{T}\right) \quad (2)$$

The fundamental absorption, which corresponds to the transition from valence band to the conduction band, can be used to determine the band gap of the materials. The relation between absorption coefficient (α) and the incident photon energy (hυ) can be written as [27].

$$\alpha h\nu = A\left(h\nu - E_g\right)^r \quad (3)$$

where A is a constant, Eg is the band gap of the material and the exponent r depends on the type of Transition. r may have values 1/2, 2, 3/2 and 3 corresponding to the allowed direct, allowed indirect, forbidden direct and forbidden indirect transitions, respectively.

Now equation (3) may be written as

$$\frac{d\left[\ln\left(\alpha h\nu\right)\right]}{d\left(h\nu\right)} = \frac{r}{\left(h\nu - E_g\right)} \quad (4)$$

The above equation indicates that the plot of d[ln(αhυ)]/d(hυ) → hυ must have a divergence at an energy value equal to Eg, where the transition takes place.

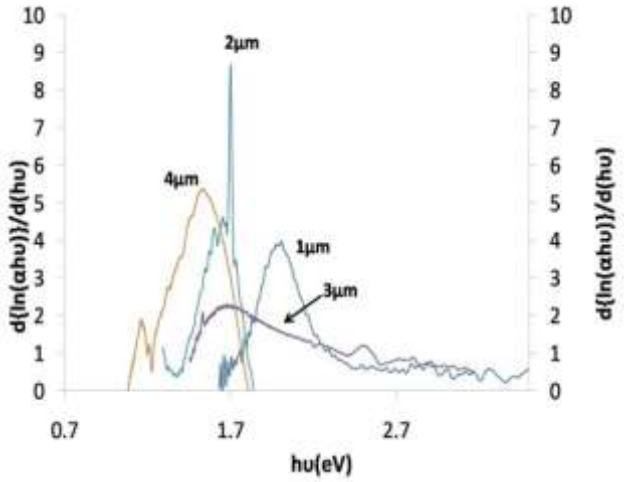

Fig. 7 Plot of d{ln(αhυ)}/d(hυ) →hυ of Nanocrystalline SnSe thin films.

Fig. 7 shows the plot of d{ln(αhυ)}/d(hυ) →hυ. We can see a discontinuity around at 2.0eV, 1.7eV,1.6eV and 1.5eV for 1µm, 2µm, 3µm and 4µm respectively. Taking this value as approximate band gap prepared thin films, ln (αhυ) → ln (hυ – Eg) graph is plotted, so that the ature of the transition (i.e. r value) can be determined.

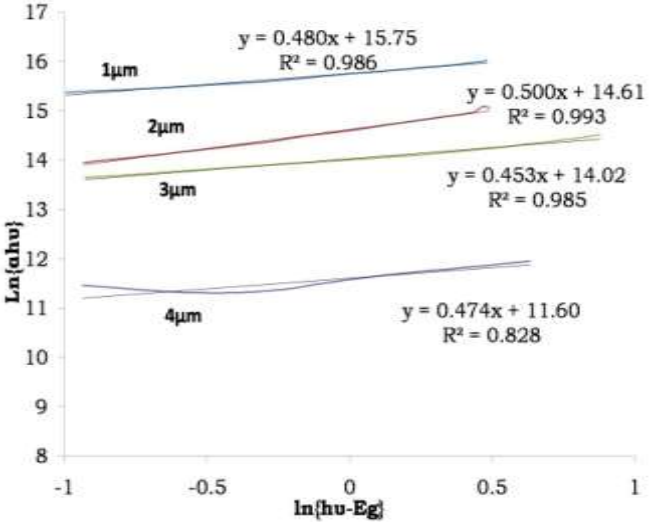

Figure 8: plot of ln (αhυ) →ln (hυ – Eg) of Nanocrystalline SnSe thin films.

From the slope of this straight line graph (Fig. 8), value of r has been calculated, which is found to be around 0.5 for all thin films indicating that the transition is direct. Using this value of r (0.5), the exact value of the band gap is calculated by extrapolating the straight line portion of the (αhυ)1/r → hυ graph to the hυ axis. Figure 9 shows the plot of (αhυ)2 → hυ.

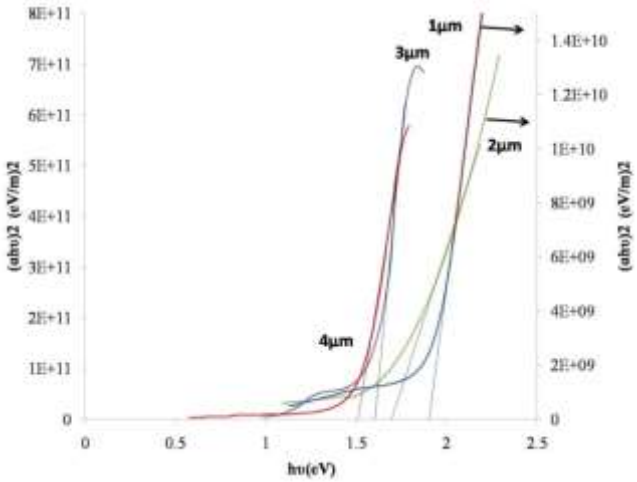

Fig. 9 Plot of $(\alpha h\upsilon)^2 \rightarrow h\upsilon$ of Nanocrystalline SnSe thin films.

The obtain value of the band gap are shown in table 3. It is observed that the value of Eg is higher than the bulk Value of SnSe (1.1eV) due to quantum confinement in thin films. The blue-shift of the band gap (Eg) can be used to calculate the average particles size using relation [28,29].

$$\Delta E_g = E_{shift} = \frac{\hbar^2 \pi^2}{2\mu R^2} \qquad (5)$$

where Eshift is the shift in the band gap, μ is the translation mass and R the radius of the nanoparticles. This formula is applicable in our case as we are well below the strong confinement regime. We have calculated the particle size of Nano crystalline SnSe thin films using equation (5) and shown in table 3 which is comparable near to XRD and TEM results.

Table 3: obtain optical band gap and particle size of Nanocrystalline SnSe thin films.

Thin films	**Optical band gap Eg (eV)**	**particle size R (nm)**
1µm	1.92	10.13
2µm	1.70	11.84
3µm	1.61	12.84
4µm	1.51	14.32

From table 3 it is observed that as thickness of deposited thin films is increased its optical band gap is decreases due to increased in particle size because of the size effect of Nanostructures. Another reason is also responsible for the change of optical band gap with thickness. It has been observed that band gap varies with thickness because of changes in the barrier height at the grain boundaries with variation of thickness, also due to high density of dislocations as we determine in XRD measurements respectively. It is proposed that charge accumulation at grain boundaries influences energy barrier associated with grain boundaries and affects the barrier height and there is a change in optical band gap with variation of film thickness.

IV. CONCLUSION

In this paper, we have reported the synthesis of nanocrystalline SnSe thin film by spin coating method and effect of thickness on structural as well as optical properties. It is found that as the thickness is increased particle size is increased. Also micro strain and optical band gap are decreased. These results shows as the thickness increased crystallanity of thin films increased. Also Quantum size effect occurs in our prepared thin films and these quantum size effect is depends thickness.

AKNOWLEDGEMENTS

Authors are thankful to SICART, V. V. Nagar, K. C. Patel R & D center, Changa and department of chemistry, SPU, V. V. Nagar for providing technical services to characterize materials

REFERENCES

[1]. B. Pejova, I. Grozdanova, (2005). Mat. Chem. Phys. **90**, 35.
[2]. V. C. Costa, Y. Shen, K. L. Bray, (2002). J. Non-Cryst. Solids **304**, 217.
[3]. S. N. Sarangi, S. N. Sahu, (2004). Physica E **23**, 459.
[4]. U. V. Desnica, I. D. Desnica-Frankovic, O. Gamulin, C. W. White, E. Sonder, R. A. Zuhr, (2002). J. Non-Cryst. Solids **299**, 1100.
[5]. L. Li, J. Hu, W. Yang, A. P. Alivisatos,(2001). Nano Letters **1**, 349.
[6]. L. E. Bruce, (1984). J. Chem. Phys. **80**, 4403.
[7]. Z. Zhang, M. Zhao, Q. Jiang, (2001). Semicond. Sci. Technol. **16**, L33.
[8]. S. B. Qadri, E. F. Skelton, D. Hsu, A. D. Dinsmore, J. Yang, H. F. Gray, B. R. Ratna, (1999). Phys. Rev. B **60**, 9191.
[9]. C. C. Chen, A. B. Herhold, C. S. Johnson, A. P. Alivisators, (1997). Science **276**, 398.
[10]. P. Nemec, D. Mikes, J. Rohovec, E. Uhlirova, F. Trojanek, P. Maly, (2000). Mat. Sci. Eng. B **69**, 500.
[11]. J. F. Suyver, R. Bakker, A. Meijerink, J. J. Kelly, (2001). Phys. Stat. Sol. (b) **224**, 307.
[12]. D. L. Kelin, R. Roth, A. K. L. Lim, A. P. Alivisatos, P. L. McEuen, (1997). Nature **389**, 699.
[13]. K. R. Murali, V. Swaminathan, D. C. Trivedi, (2004). Sol. Energy Mat. Sol. Cells **81**, 113.
[14]. Z. Nabi, A. Kellou, S. Me´c¸abih, A. Khalfi, N. Benosman, (2003). Mater. Sci. Eng. B 98 104.
[15]. Y. Hua, W. Chen, J.F. Chen, S. Zhang, (2003). Mater. Lett. 57 3137.
[16]. H. Ebe, F. Sakuraia, Z.Q. Chend, A. Uedonod, B.-P. Zhange, Y. Segawae, K. Sutoa, J.-i. Nishizawa, (2002). J. Cryst. Growth 237–239 1566.
[17]. Y.-l. Yan, Y. Li, X.-f. Qian, J. Yin, Z.-k. Zhu, (2003). Mater. Sci. Eng. B 103 202.
[18]. M. Sotelo-Lerma, R.A. Zingaro, S.J. Castillo, (2001). J. Organomet. Chem 623 81.

[19]. A.P. Belyaev, V.P. Rubets, M.Yu. Nuzhdin, (2003). Semiconductors 37 646.
[20]. W. Zhang, Z. Yang, J. Liu, Y. Qian, W. Yu, Y. Jia, X. Liu, G. Zhou, J. Zhu, (2001). J. Solid State Chem. 161 184.
[21]. S. Schlecht, M. Budde, L. Kienle, (2002). Inorg. Chem. 41 6001.
[22]. Q. Han, Y. Zhu, X. Wang, W. Ding, (2004). J. Mater. Sci. 39 4643.
[23]. Z. Zainal, S. Nagalingam, A. Kassim, M.Z. Hussein, W.M.M. Yunus, (2004). Solar Energy Mater. Solar Cells 81 261.
[24]. K. Zweibel, (2000). Solar Energy Mater. Solar Cells 63 375.
[25]. C. Wang, Y. D. Li, G. H. Zhang, J. Zhuang, G. Q. Shen, (2000). Inorg. Chem. 39, 4237-4239.
[26]. P. Scherrer, (1918). Mathematisch-Physikalische Klasse 2, 98-100.
[27]. J. I. Pankove, (1971). Optical Processes in Semiconductors, Englewood Cliffs. NJ: Prentice-Hall. Efros, A. L. Efros, (1982). Sov. Phys. Semicond. **16**, 772.
[28]. W. Wei-Yu, J. N. Schulman, T. Y. Hsu, Feron Uzi, (1987). Appl. Phys. Lett. **51**, 710.